other words, it serves as a M2BP glycosylation isomer (M2BPGi) for estimating the progression level of fibrosis. We validated the correlation of FastLec-Hepa counts with the degree of fibrosis using samples from 209 patients with chronic hepatitis (CH) at two locations and documented its possible clinical utility for evaluating therapy by quantifying the degree of disease severity. In particular, the count-dependent monitoring for long-term follow-up (up to 3 years) of severely affected patients with any antiviral treatments was considered to be effective in the prevention of liver-related morbidity and mortality such as hepatic decompensation and hepatocellular carcinoma. To achieve the continuous monitoring based on the "on-site measurement", the assay must be standardized and the obtained counts should be normalized with an appropriate COI value. These might also achieve standardization in measuring disease severity and planning therapies. From these viewpoints, we decided that our validated FastLec-Hepa assay could be reconstructed effectively (see the final step of the developmental pipeline shown in Supporting Information Fig. S1) by creating a reliable calibrator.

In principle, as FastLec-Hepa monitors the level of fibrosis-related hM2BPGi, it requires an assay calibrator with dual epitopes: a glycan that is recognized by

WFA and an hM2BP peptide that reacts to an anti-hM2BP monoclonal antibody (mAb). Recombinant proteins for use as assay calibrators are generally produced in bacterial or yeast expression systems because of their high productivity and cost-effectiveness. However, these were not suitable for our purpose as the recombinant proteins produced from bacterial cells had no glycans and those from yeast cells contained only high mannose-type glycans, neither recognized by WFA. In our system, a mammalian cell line exhibiting WFA positivity was needed to produce the recombinant hM2BP (rhM2BP) as the assay calibrator. It was important to select a suitable host cell line for expressing rhM2BP because WFA positivity for hM2BP would depend on the glycosynthetic machinery of each cell line. To select host cells with prominent WFA reactivity, we first conducted a lectin microarray analysis on culture supernatants from two mammalian cell lines (Supporting Information Fig. S2), Chinese hamster ovary (CHO) cells and human embryonic kidney (HEK293) cells, both of which are popular for producing recombinant proteins. Both cell lines were obtained from the American Type Culture Collection (Manassas, VA) and were cultured in DMEM and RPMI-1460 medium (Gibco, Grand Island, NY) without FCS for 48 h. In the lectin microarray analysis under the direct-labeling method with Cy3, the culture supernatant of the

HEK293 cells exhibited higher WFA signals than that of the CHO cells (Fig. 1A). This result indicated that HEK293 cells had the potential to produce glycoproteins with higher WFA reactivity. Regarding the culture conditions, the lectin microarray also showed that DMEM was more suitable for a high WFA response than RPMI-1460 (Fig. 1A). Therefore, we finally established a stable cell line using HEK293 cells as a host.

To confirm the WFA positivity of rhM2BP expressed by HEK293 cells and to determine the interlot variability of production simultaneously, rhM2BP was subsequently expressed in HEK293 cells four times on different days and purified twice from each culture medium (Supporting Information Fig. S3 and Methods). A comparative glycan profiling of rhM2BP with signal intensities of the lectin microarray suggested WFA-positivity for rhM2BP without remarkable difference among the eight purification variants (Fig. 1B). Focusing on the WFA signals showing slight differences in intensity (CV = 15.7%, in the *left* panel of Fig. 1C), which might be attributed to variability in protein concentration, we further qualified the reactivity of each sample against WFA on the lectin microarray using data processing as described previously [12]. In this case, it would be appeared as a quantitative difference in rhM2BP in the level of a terminal Gal/GalNAc

marker of *N*-glycan, one of the WFA ligands [8]. The rate of produced asialo form shows an almost negative correlation with the ratio of sialylation. Therefore, data processing using the 6′-sialyllactosamine-binding lectin from *Sambucus sieboldiana* (SSA) as a normalizer enabled the precise qualification of WFA reactivity. As we expected, the result suggested that there was no qualitative difference among the production lots of rhM2BP in terms of the amount of the WFA ligand (CV = 5.6%, see the *right* panel of Fig 1C). Collectively, we constructed the protocol for production of rhM2BP as the assay calibrator.

We next examined the construction of an anti-rhM2BP mAb optimized for the sandwich immunoassay. Mice were immunized with rhM2BP and 13 productive mAb clones were selected based on their productivity and reactivity against rhM2BP. The mAb produced from each clone was purified (Supporting Information Fig. S4) and then biotinylated. Biotinylated mAb (25 ng per assay) was overlaid on the lectin microarray that had been incubated with rhM2BP overnight. The suitability of each mAb as the detecting antibody was assessed from the signal-to-noise ratio in the lectin–antibody sandwich immunodetection system (Supporting Information Figs S5 and S6). As a result, all mAb clones except for No. 2, with a high signal-to-noise ratio, were selected at this step. After

absence of potential interaction of HRP with WFA was confirmed (Supporting Information Fig. S7), the reactivity of each mAb clone against WFA-binding rhM2BP was further qualified in the HRP-assisted sandwich ELISA using a microtiter plate (Fig. 2A and Supporting Information Methods). Two clones (Nos. 11 and 28) were selected as the most feasible detection antibody along with a conventional accelerated stability test (Fig. 2B). In the following spiking experiment with rhM2BP (see Supporting Information Methods), we finally concluded that clone No. 28 was the best mAb with resistance against inactivation of the antigen–antibody reaction by serum components (Fig. 2C).

We prepared our diagnostic agent for the direct measurement of serum WFA^+-hM2BP with this antibody. To examine for variations, we performed triplicate measurements for rhM2BP on different days and different production lots. The intraday variations in measurements indicated high reproducibility of the assay (CV = 1.3, 0.7 and 2.3%) using the fully automatic immunoanalyzer HISCL-2000i (Sysmex Co., Hyogo, Japan), whereas the overall difference among the lots was not minimized (CV = 10.4%). Therefore, we reduced the interday and lot variations by indexing the measured values with the value of an exact amount of rhM2BP as a calibrator in the following procedure.

1. The mean +2.5 SD value of the measured values of 800 samples arbitrarily selected from the data set of sera from 1000 healthy volunteers (HV) that we recently reported [8] was assigned as a COI of 1.0 (Fig. 3).
2. An rhM2BP solution was prepared at a concentration to yield this COI value. This solution was designated as the master calibration solution for future production.
3. This calibrator used as a positive control and the buffer as a negative control was measured at least three times for each run of the HISCL-2000i.
4. The measured values (WFA^+-hM2BP) were indexed with the obtained values using the following equation:

   $COI = ([WFA^+\text{-hM2BP}]_{sample} - [WFA^+\text{-hM2BP}]_{NC}) / ([WFA^+\text{-hM2BP}]_{PC} - [WFA^+\text{-hM2BP}]_{NC})$

   $[WFA^+\text{-hM2BP}]_{sample}$, WFA^+-hM2BP count of serum sample (PC, positive control; NC, negative control).

As a result, the mean was 377710, the SD 272230, and the mean +2.5 SD value 1058285. Reliability was then validated using the remaining samples, where the number of samples having COI >1 was 10 out of 200 (5.0% of the total).

Subsequently, we evaluated the reconstructed system with the data set from our previous study [8]. A total of 232 samples from 3 different sites had been measured without dilution (direct measurement) and after 10-fold dilution, of which 117 HV samples were measured on different days with the kits of different production lots and 114 CH samples on the same day with the same production lot (1 CH sample was excluded as the direct measurement exceeded the LOQ). In the resulting 2D plots, both slopes were approximated at 0.96 with high correlation coefficients (R^2 = 0.98 and 0.99). For clinical use, the COI would help in understanding disease severity. The significance of the COI is currently under validation using over 10,000 samples from 15 different sites. The validation will not only support reliability of the glycodiagnostic agent, but also provide advantageous information on basic science, enabling the focused glycoproteomics with well-defined target cases and controls to clarify the structure of the disease-related glyco-alterations on M2BP. Further experiments for glycoproteomics and molecular pathology of M2BP will elucidate the mechanism of M2BP with such glyco-alterations secreted into serum.

In conclusion, we have reconstructed our sandwich assay system as a robust diagnostic agent thanks to the development of a robust calibrator. This was

achieved using the evidence-based technology of lectin-assisted glycan profiling focusing on cell-to-cell and protein-to-protein glyco-alterations. Our development pipeline is highly efficient and applicable to a wide variety of glycodiagnostic agents and might accelerate the incorporation of glycan-based technologies into the clinical arena.

We thank A. Togayachi, H. Kaji, A. Takahashi (AIST) and Y. Hamaguchi, T. Kagawa, S. Nagai, S. Matsubara, M. Terao (Sysmex Co.) for technical assistance, critical suggestions on assay development, or critically reading our manuscript. This work was supported in part by a grant from New Energy and Industrial Technology Development Organization of Japan.

The authors have declared no conflict of interest.

References

[1] Taniguchi, N., Hancock, W., Lubman, D. M., Rudd, P. M, The second golden age of glycomics: from functional glycomics to clinical applications. *J. Proteome Res.* 2009, *8*, 425–426.

[2] Sato, Y., Nakata, K., Kato, Y., Shima, M., *et al.*, Early recognition of hepatocellular-carcinoma based on altered profiles of alpha-fetoprotein. *N. Eng. J. Med.* 1993, *328*, 1802–1806.

[3] Rifai, N., Gillette, M.A., Car, S.A., Protein biomarker discovery and validation: the long and uncertain path to clinical utility. *Nat. Biotech.* 2006, *8*, 971–976.

[4] Narimatsu, H., Sawaki, H., Kuno, A., Kaji, H.*et al.*, A strategy for discovery of cancer glyco-biomarkers in serum using newly developed technologies for glycoproteomics. *FEBS J.* 2010, *277*, 95–105.

[5] Kagebayashi, C., Yamaguchi, I., Akinaga, A., Kitano, H., *et al.*, Automated immunoassay system for AFP-L3% using on-chip electrokinetic reaction and separation by affinity electrophoresis. *Anal. Biochem.* 2009, *388*, 306–311.

[6] Callewaert, N., Van Vlierberghe, H., Van Hecke, A., Laroy, W., *et al.*,

Noninvasive diagnosis of liver cirrhosis using DNA sequencer-based total serum protein glycomics. *Nat. Med.* 2004, *10*, 429–434.

[7] Haab, B. B., Using lectins in biomarker research: Addressing the limitations of sensitivity and availability. *Proteomics Clin. Appl.* 2012, *6*, 346–350.

[8] Kuno, A., Ikehara, Y., Tanaka, Y., Ito, K., *et al.*, A serum "sweet-doughnut" protein facilitates fibrosis evaluation and therapy assessment in patients with viral hepatitis. *Sci. Rep.* 2013, *3*, 1065.

[9] Chen, S., LaRoche, T., Hamelinck, D., Bergsma, D., *et al.*, Multiplexed analysis of glycan variation on native proteins captured by antibody microarrays. *Nat. Methods* 2007, *4*, 437–444.

[10] Korekane, H., Hasegawa, T., Matsumoto, A., Kinoshita, N., *et al.*, Development of an antibody-lectin enzyme immunoassay for fucosylated α-fetoprotein. *Biochim. Biophys. Acta* 2012, *1820*, 1405–1411.

[11] Kuno, A., Kato, Y., Matsuda, A., Kaneko, M. K., *et al.*, Focused differential glycan analysis with the platform antibody-assisted lectin profiling for glycan-related biomarker verification. *Mol. Cell. Proteomics* 2009, *8*, 99–108.

[12] Kuno, A., Ikehara, Y., Tanaka, Y., Angata, T., *et al.*, Multilectin assay for

detecting fibrosis-specific glyco-alteration by means of lectin microarray. *Clin. Chem.* 2011, *57*, 48–56.

[13] Kuno, A., Uchiyama, N., Koseki-Kuno, S., Ebe, Y., *et al.*, Evanescent-field fluorescence-assisted lectin microarray: a new strategy for glycan profiling. *Nat. Methods* 2005, *2*, 851–856.

Figure 1. Efficient construction of WFA-positive rhM2BP as a calibrator for a quantitative lectin–antibody sandwich immunoassay. Cell glycomes of culture supernatants of CHO and HEK293 cells cultivated in RPMI or DMEM were analyzed using a 45-lectin microarray (A). The obtained signal intensity was normalized against the means of signals on the 45 lectins. The asterisk indicates the signal intensity of WFA. (B) Comparative analysis of glycan profiles among four different rhM2BP production lots. Respective glycan profiles of two purification samples per production lot were averaged and are represented as a bar graph with error bars. The reactivity to WFA is displayed separately in the *left* panel of (C). The interlot variability on the WFA reactivity was further estimated by standardizing the signal on WFA using SSA in the *right* panel of (C).

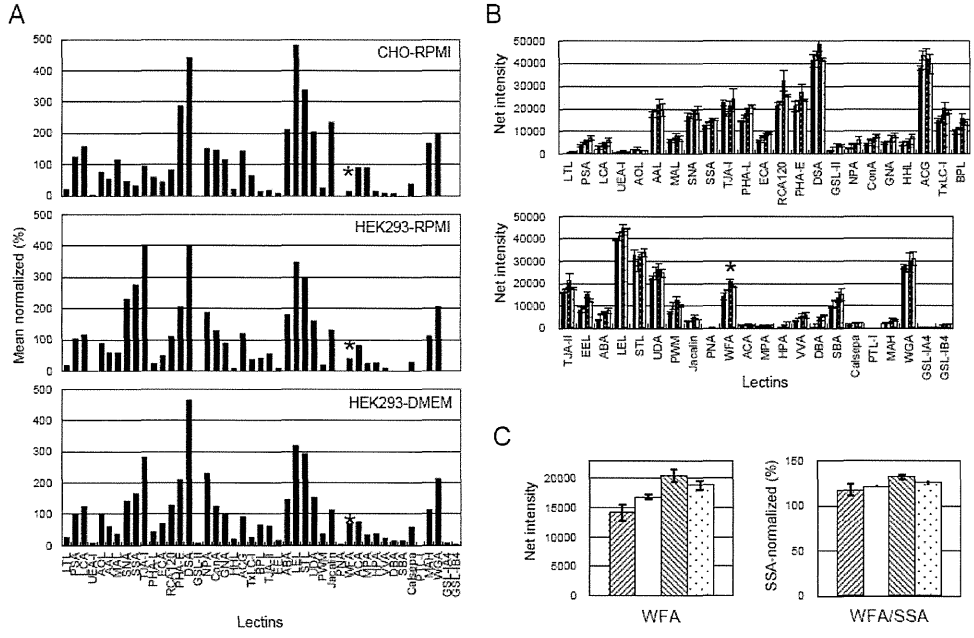

Figure 2. Sequential screening of the most reliable anti-hM2BP mAb using a lectin microarray with twofold serial dilution in a WFA–antibody sandwich ELISA (A), accelerated stability test (B) and spiking experiment (C). In the spiking experiment, appropriate amounts of rhM2BP were dissolved in the reaction buffer in the presence (open squares) or absence (closed squares) of serum samples where endogenous hM2BP had been depleted by immunoprecipitation.

A

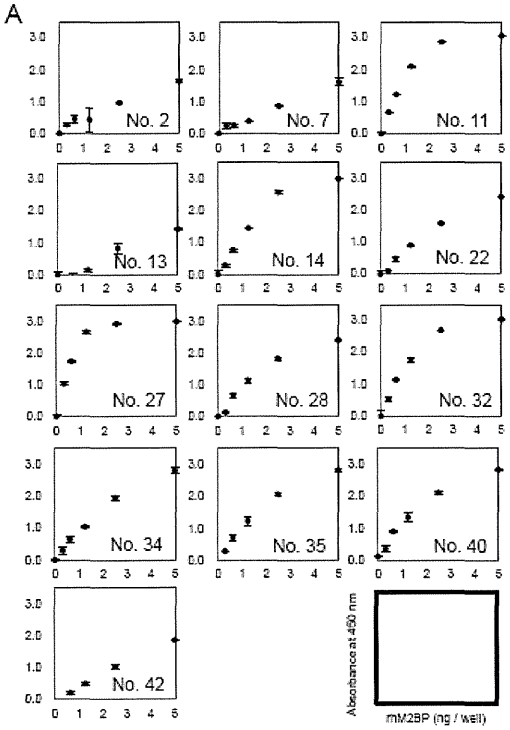

B

Clone No.	IgG subclass	Stability (%)			
		Serum A		Serum B	
		Day 7	Day 14	Day 7	Day 14
2	IgG1	83	75	84	77
7	IgG1	83	73	85	76
11	IgG2a	94	82	100	87
13	IgG1	92	81	89	84
14	IgG1	87	73	90	77
22	IgG1	95	86	92	82
27	IgG2a	86	72	82	74
28	IgG1	93	80	95	85
32	IgG1	85	77	84	73
34	IgG1	79	75	79	72
35	IgG1	77	73	80	70
40	IgG1	93	77	96	83
42	IgG1	81	72	82	74

C

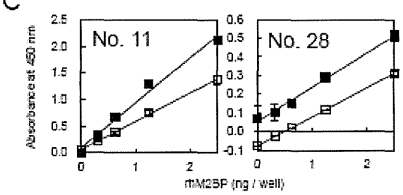

Figure 3. Cutoff index (COI) values for standardization of WFA^+-hM2BP counts showing the distribution of WFA^+-hM2BP counts of 800 samples from healthy volunteers.

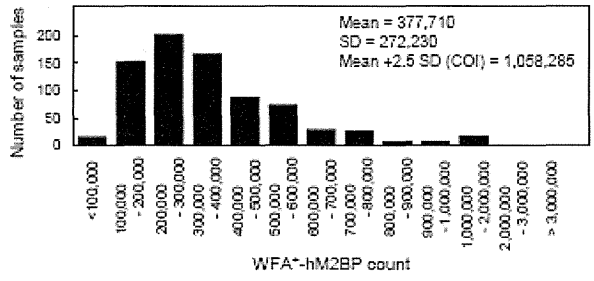

Pathology International

Pathology International 2013; **63**: 305–310 doi:10.1111/pin.12064

Original Article

Quantification of collagen and elastic fibers using whole-slide images of liver biopsy specimens

Tokiya Abe,[1] Akinori Hashiguchi,[1] Ken Yamazaki,[1] Hirotoshi Ebinuma,[2,3] Hidetsugu Saito,[2,3] Hiromitsu Kumada,[4] Namiki Izumi,[5] Naohiko Masaki[6] and Michiie Sakamoto[1]

Departments of [1]Pathology and [2]Internal Medicine, School of Medicine, and [3]Faculty of Pharmacy, Keio University, [4]Department of Gastroenterology, Toranomon Hospital, [5]Department of Gastroenterology and Hepatology, Musashino Red Cross Hospital, Tokyo and [6]The Research Center for Hepatitis and Immunology, National Center for Global Health and Medicine, Chiba, Japan

Histological evaluation of fibrosis after a liver biopsy is crucial for evaluating the pathology of patients with chronic liver disease. Previous studies have reported quantitative analyses of fibrosis using images of collagen-stained sections. However, analysis of these studies requires manual selection of the region of interest. In addition, the quantification of elastic fibers is not considered. The present study was conducted in order to measure both the collagen and elastic fiber area ratios using Elastica van Gieson-stained whole-slide images (WSIs) of liver biopsy specimens. High-resolution WSIs provide precise color classification, enabling accurate detection of even fine collagen and elastic fibers. To minimize the influence of pre-existing fibrous tissue, median area ratios of the collagen and elastic fibers were independently calculated from the image tiles of the WSIs. These median area ratios were highly concordant with area ratios after the pre-existing fibrous tissues were manually trimmed from the WSI. Further, these median area ratios were correlated with liver stiffness as measured by transient elastography (collagen: $r = 0.73$ [$P < 0.01$], elastic: $r = 0.53$ [$P < 0.01$]). Our approach to quantifying liver fibrosis will serve as an effective tool to evaluate liver diseases in routine practice.

Key words: collagen, computer-assisted image analysis, elastin, elastography, liver fibrosis, whole-slide image

Evaluation of liver fibrosis in patients with chronic liver disease is crucial for understanding the disease state, predicting prognosis and selecting the appropriate treatment.[1,2] Although the efficacy of biochemical methods[3–6] and transient elastography for measuring liver stiffness[7] has been demonstrated, histopathological evaluation of liver biopsy specimens remains the gold standard. At present, histopathological evaluation of fibrosis using liver biopsy specimens is performed by a pathologist who stages specimens by identifying the location, degree and pattern of fibrosis, presence of architectural distortion, and regenerative nodule formation. This staging is completely dependent on the experience of the observer, and there is intra- as well as inter-individual variation in this respect.[1] To overcome these issues, quantification by imaging analysis has been suggested for evaluating the degree of liver fibrosis.[8–17] In these studies, collagen fibers were extracted from the histological image of the liver biopsy specimen, and the area occupied by the fibers relative to the area of the entire tissue specimen was quantified as a ratio. However, most of the proposed quantification methods still need an observer to define the region of interest or trim pre-existing fibrous tissue such as skin, muscle, or a large blood vessel.[8–14] An increase in collagen deposition is involved in the progression of liver fibrosis. Deposition of elastic fibers is also reportedly increased, particularly in late stages of the disease.[18–21] Thus, evaluation of elastic as well as collagen fiber deposition is crucial for the accurate evaluation of fibrosis progression; however, to our knowledge, no method that simultaneously quantifies both fibers has been reported to date.

The whole-slide imaging system, which is popular in telepathology and education, enables an entire tissue section to be digitized at a high resolution within minutes and saved as a whole-slide image (WSI).[22–24] Once the WSI is stored as digital data, it is easy to obtain individual pixel color values, and WSIs can be used for several applications including morphometrical analysis.[25–28] The purpose of this study is to develop an effective method to quantify liver fibrosis using

Correspondence: Michiie Sakamoto, MD, PhD, Department of Pathology, School of Medicine, Keio University, 35 Shinanomachi, Shinjuku-ku, Tokyo 160-8582, Japan. Email: msakamot@z5.keio.jp

Received 24 January 2013. Accepted for publication 2 May 2013.

the WSIs of liver biopsy specimens. We established a method that simultaneously quantifies the collagen and elastic fiber area ratios in Elastica van Gieson (EVG)-stained liver biopsy tissue specimens. Further, the area ratios were compared with liver stiffness as measured by transient elastography. This method of quantifying liver fibrosis using WSIs may become important in the future as a technique for assisting with pathological diagnosis.

METHODS

Samples

Liver biopsy specimens were collected from 38 chronic viral hepatitis patients (37 with chronic hepatitis C virus, and one with chronic hepatitis B virus) from four medical facilities. After obtaining the informed consent, we measured the liver stiffness by using FibroScan (Echo-Sens, Paris, France). The stiffness of the right lobe of the liver was measured by placing a probe tip into the intercostal space at a depth of 2.5–6 cm from the skin surface. Liver stiffness was measured 10 times, and the median value of these 10 measurements was used for each patient.

EVG staining

The liver biopsy specimens were formalin-fixed and paraffin-embedded. The specimens were then sliced to a thickness of 3 μm and stained with EVG. A WSI of each specimen was acquired using the NanoZoomer 2.0HT (Hamamatsu Photonics K.K., Hamamatsu, Japan) at a × 20 objective lens equivalent to 0.46 μm/pixel.

Quantification of fibrosis using WSI analysis

The WSI pixels were classified into five classes corresponding to four tissue components: collagen fibers, elastic fibers, nucleus, cytoplasm, and one non-tissue component (i.e. glass slide). The training data points, which were extracted from the portal and periportal areas in the WSI, were sampled for at least 30 points for each class. The color distributions of the five classes were analyzed in RGB color space, wherein the color analyses were done for all specimens. Subsequently, a quadratic discriminant function based on the color distribution[29] was applied in order to label each WSI pixel appropriately.

The area ratio of each tissue component is the sum of pixels for each tissue component divided by the total number of pixels of the four tissue components. The median area ratios of collagen and elastic fibers were also calculated. An image-processing program was developed using MATLAB (The MathWorks, Inc., Natick, MA, USA) for image analysis.

Statistical analysis

Relationships between measurement values were analyzed using the Spearman's rank correlation coefficient test. All *P*-values were two-tailed, and values less than 0.05 were considered statistically significant. Analyses were carried out using SPSS software (version 19.0; SPSS Inc., Chicago, IL, USA).

RESULTS

The evaluated liver biopsy specimens had an average length of 16.3 mm (SD = 3.2 mm) and an average width of 1.0 mm (SD = 0.3 mm). This is equivalent to an average of 77 mega-pixels (SD = 36 mega-pixels) in WSIs. The time required for analysis was approximately 6.3 min (SD = 3.3 min) per biopsy specimen.

Color classification of EVG-stained tissue specimens

The training data points for five classes were from the portal and periportal areas on the WSI of EVG-stained liver biopsy specimens (Fig. 1a). The extracted training data points were plotted in RGB color space (Fig. 1b). Five classes of the data points in all liver biopsy specimens were individually distinguishable in the three-dimensional color space. The composition of the color distribution of the five classes was different among the biopsy specimens, therefore, the quadratic discriminant function was designed based on the training data points in each liver biopsy specimen and applied to determine the color classification of the pixels. As a result, every pixel on the WSIs of all liver biopsy specimens was successfully labeled in the appropriate classes (Figs S1,S2). Figure 2 shows that even fine collagen and elastic fibers could be extracted from portal and periportal areas.

Measurements of the area ratios of tissue components on WSIs

The area ratio of each tissue component could be calculated from the labeled pixels. The average area ratios of collagen, elastic fibers, nucleus and cytoplasm in all biopsy specimens were 11.3% (SD = 5.1%), 3.8% (SD = 2.7%), 11.8% (SD = 5.0%) and 73.1% (SD = 8.7%), respectively. Representative WSIs and classification results of liver biopsy specimens with mild fibrosis and severe fibrosis are shown in

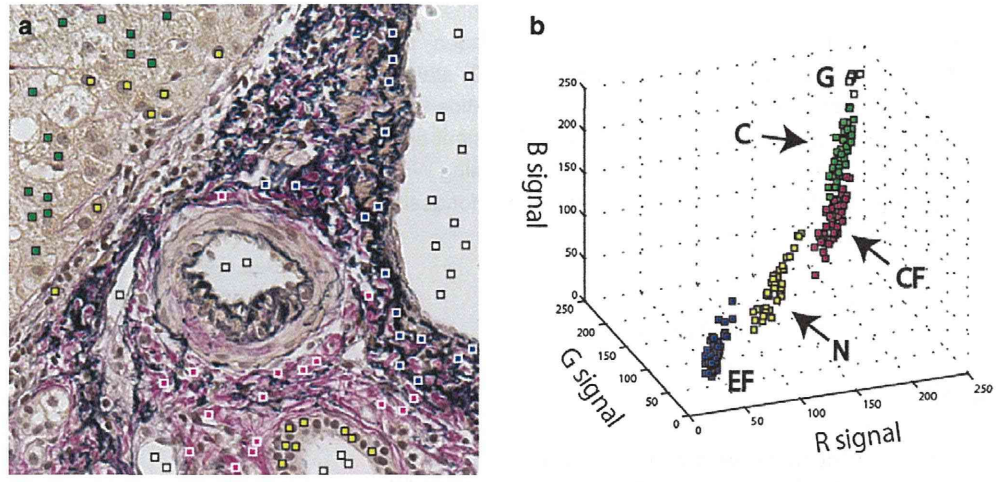

Figure 1 Sampling and color distribution. (**a**) Colored squares indicate training data points for five classes in the portal and periportal area (250 × 250 μm²). (**b**) Color distribution of the data points in RGB color space. Each color represents a class: collagen fiber (CF), red; elastic fibers (EF), blue; cell nuclei (N), yellow; cytoplasm (C), green; glass slide (G), white.

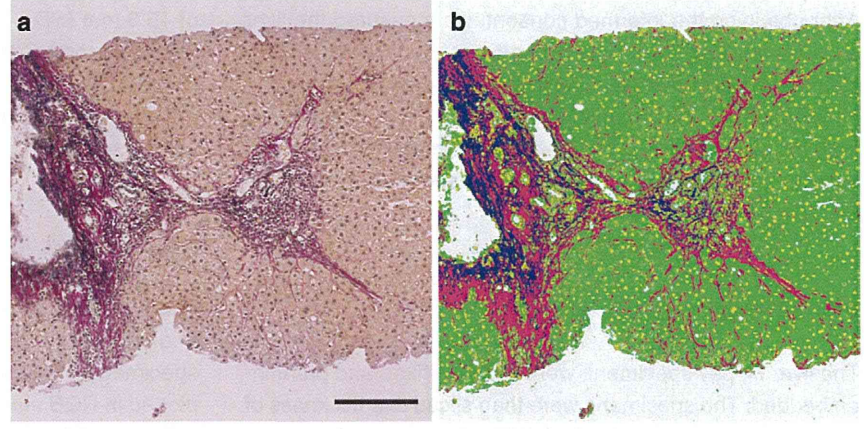

Figure 2 Color image and classification result in the portal and periportal areas (1 × 1 mm²). In the color classification result, collagen fibers, elastic fibers, nuclei, cytoplasm, and glass slide were red, blue, yellow, green, and white, respectively. Scale bar, 0.2 mm.

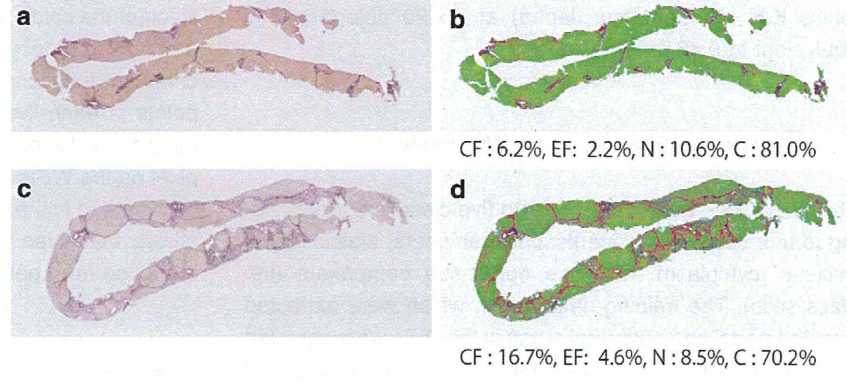

Figure 3 Measurements of area ratio on the whole-slide image. Representative whole slide images (WSIs) and classification results of liver biopsy specimen with mild fibrosis (**a,b**) and with severe fibrosis (**c,d**). The percentage indicates area ratio of each tissue component.

Figure 3a–d. The area ratios of collagen, elastic fibers, nucleus, and cytoplasm were 6.2%, 2.2%, 10.6%, and 81.0%, respectively, for mild fibrosis. The area ratios for severe fibrosis were 16.7%, 4.6%, 8.5%, and 70.2%, respectively. The area ratios of collagen as well elastic fibers were higher for patients with severe fibrosis than for those with mild fibrosis.

Median area ratios of collagen and elastic fibers

Previous papers reported that pre-existing fibrous tissue, such as muscle and large blood vessels (enclosed by the dotted line in Fig. 4a), should be trimmed from the WSI prior to implementing image analysis.[8,9] The measurements show that without trimming the pre-existing fibrous tissue,

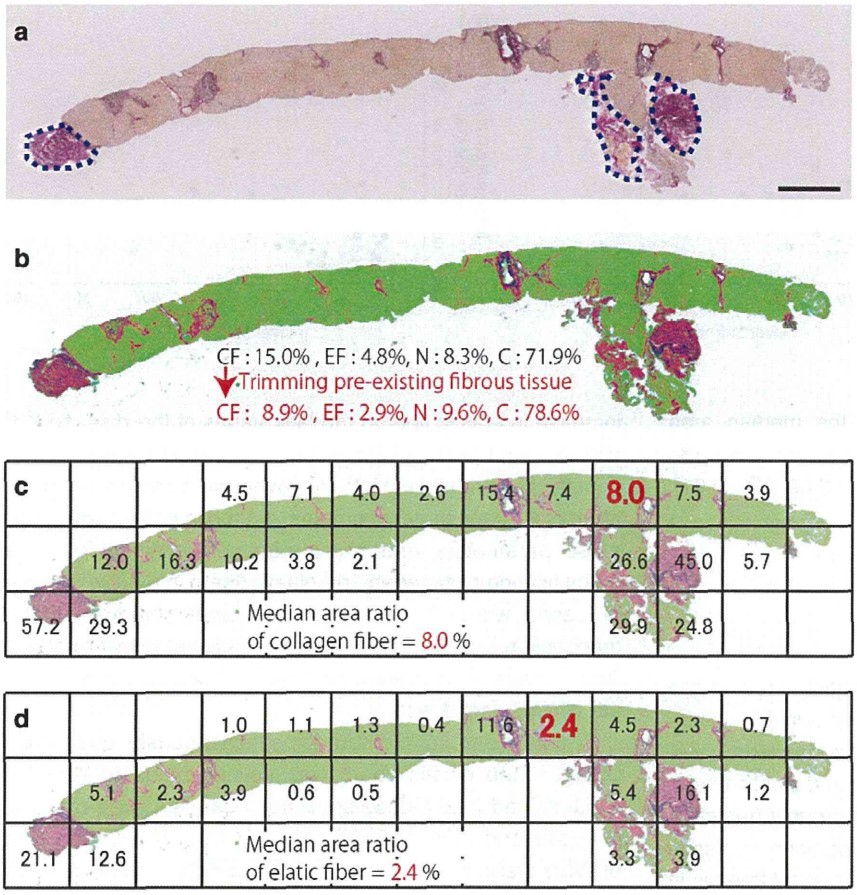

Figure 4 Median area ratios of collagen and elastic fibers. (**a,b**) Whole-slide image (WSI) and classification result of the liver biopsy specimen with mild fibrosis. (**c,d**) Median area ratios of collagen and elastic fibers, respectively, when the classification result was divided into 1×1 mm^2. Black numbers indicate area ratios of each fiber for any tiles where the tissue area occupied at least 20% of the tile area. The red number was the median area ratio of each fiber. Scale bar, 1 mm.

Table 1 Correlation between the median area ratio and area ratio after trimming the pre-existing fibrous tissue from the whole slide image

Tile size (mm^2)	0.01^2	0.25^2	0.50^2	0.75^2	1.00^2	1.25^2	1.50^2
Spearman's rank correlation coefficient							
Collagen fiber	0.79**	0.94**	0.98**	0.97**	0.98**	0.95**	0.93**
Elastic fiber	0.59**	0.87**	0.93**	0.93**	0.95**	0.92**	0.88**

**$P < 0.01$.

the area ratios of collagen and elastic fibers were 15.0% and 4.8%, respectively. After trimming, the area ratios of collagen and elastic fibers were 8.9% and 2.9%, respectively (Fig. 4b).

We then calculated the median area ratios of collagen and elastic fibers from the image tiles of WSI (Fig. 4c,d). The WSI was divided into small tiles of 1×1 mm^2. Then area ratios of each fiber on any tile, where the tissue area occupied at least 20% of the tile area, was calculated. The median area ratios of collagen and elastic fibers were determined as 8.0% (Fig. 4c) and 2.4% (Fig. 4d), respectively.

In order to determine the appropriate tile size, correlation between the median area ratios in other tile sizes and the area ratio after trimming were evaluated for all 38 liver biopsy specimens (Table 1). When the tile size was 1×1 mm^2, the median area ratios of the fibers correlated with the area ratio after trimming most strongly.

Relationship between the area ratio of fiber and liver stiffness

Correlation between the median area ratio of each fiber and liver stiffness measured by transient elastography was evaluated (Fig. 5a,b). Liver stiffness correlated well with the median area ratios of both types of fibers using a tile size of 1×1 mm^2 (collagen fiber: $r = 0.73$ [$P < 0.01$]; elastic fiber: $r = 0.53$ [$P < 0.01$]), as well as the area ratios after trimming pre-existing fibrous tissue off from WSI (collagen fiber: $r = 0.73$ [$P < 0.01$], elastic fiber: $r = 0.51$ [$P < 0.01$]). Liver

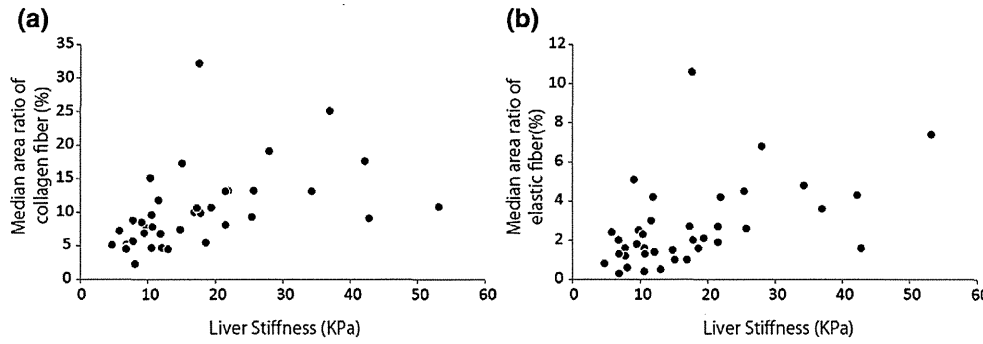

Figure 5 Scatter plot of liver stiffness by transient elastography versus median area ratios of (**a**) collagen and (**b**) elastic fibers. The tile size was 1 × 1 mm^2 when calculating the median area ratios of both fibers.

stiffness showed better correlation with the median area ratios of both fibers than with the area ratios including pre-existing fibrous tissue (collagen fiber: $r = 0.62$ [$P < 0.01$], elastic fiber: $r = 0.44$ [$P < 0.01$]).

DISCUSSION

Our color classification technique successfully labeled the WSI pixels of EVG-stained liver biopsy specimens in the appropriate classes (collagen, elastic fibers, nucleus, cytoplasm, and glass slide). Even fine collagen and elastic fibers, associated with chronic hepatitis, were accurately detected. Our results suggest that the precise recognition of tissue components in WSIs could identify not only portal fibrosis in patients with chronic viral hepatitis, but also fine pericellular fibrosis in those with alcoholic and non-alcoholic fatty liver diseases.

Pre-existing fibrous tissue such as skin, muscle and large blood vessel affects the accuracy of liver fibrosis measurements.[8] Previous studies have reported that the area ratio of collagen fiber was calculated after trimming pre-existing fibrous tissue from WSI.[8,9] Our study indicates that the trimming step could be avoided by calculating the median area ratios of collagen and elastic fibers from the image tiles of WSI. This approach can minimize the human factor and serve to establish an objective and automated quantification method. This type of image processing is one of the advantages of WSI analysis. We believe that more beneficial and useful algorithms will be developed in the near future.

Liver stiffness measured by transient elastography has been reported to correlate with the liver fibrosis stages.[7] Our results show that liver stiffness had a better correlation with the median area ratios of fibers than with the area ratios of fibers, including pre-existing fibrous tissue. This result suggests that the median area ratio of each fiber increases the correlation with liver stiffness and reflects the progression of liver fibrosis quantitatively. The liver stiffness, especially, correlated better with the median area ratio of collagen fiber than with the median area ratio of elastic fiber, probably due to an increase in elastic fiber in the late stages of the disease.[19–21] It is also possible that liver stiffness may relate to the width or density of fibrous septa.[30] However, we need to integrate other algorithms or densitometric method in order to measure those parameters and illuminate their relationships. The quantification of collagen and elastic fibers in a large number of cases would contribute to the understanding of the mechanism of fibrosis progression associated with chronic liver disease with different etiology, and would help to evaluate clinical usefulness.

In conclusion, a method for simultaneously quantifying collagen and elastic fibers was developed using WSIs of EVG-stained liver biopsy specimens. Median area ratios of collagen and elastic fibers obtained from the image tiles of WSIs were found to be correlated with liver stiffness measured by transient elastography. This enabled more accurate quantification of liver fibrosis than the area ratio of each fiber, including pre-existing fibrous tissue. Our approach of quantifying liver fibrosis will serve as a useful tool to effectively evaluate liver diseases in routine practice.

ACKNOWLEDGMENTS

This study was supported by the New Energy and Industrial Technology Development Organization (NEDO). The authors thank K. Effendi, M. Iwata, M. Takeichi, Y. Nagafuji, and Y. Hashimoto for technical assistance.

REFERENCES

1 The French METAVIR Cooperative Study Group. Intraobserver and interobserver variations in liver biopsy interpretation in patients with chronic hepatitis C. *Hepatology* 1994; **20**: 15–20.
2 Desmet VJ, Knodell RG, Ishak KG *et al.* Formulation and application of a numerical scoring system for assessing histological activity in asymptomatic chronic active hepatitis [Hepatology 1981; 1: 431–435]. *J Hepatol* 2003; **38**: 382–6.
3 Koda M, Matunaga Y, Kawakami M, Kishimoto Y, Suou T, Murawaki Y. FibroIndex, a practical index for predicting significant fibrosis in patients with chronic hepatitis C. *Hepatology* 2007; **45**: 297–306.

4 Forns X, Ampurdanes S, Llovet JM *et al.* Identification of chronic hepatitis C patients without hepatic fibrosis by a simple predictive model. *Hepatology* 2002; **36**: 986–92.
5 Wai CT, Greenson JK, Fontana RJ *et al.* A simple noninvasive index can predict both significant fibrosis and cirrhosis in patients with chronic hepatitis C. *Hepatology* 2003; **38**: 518–26.
6 Ngo Y, Munteanu M, Messous D *et al.* A prospective analysis of the prognostic value of biomarkers (FibroTest) in patients with chronic hepatitis C. *Clin Chem* 2006; **52**: 1887–96.
7 Ebinuma H, Saito H, Komuta M *et al.* Evaluation of liver fibrosis by transient elastography using acoustic radiation force impulse: Comparison with Fibroscan ®. *J Gastroenterol* 2011; **46**: 1238–48.
8 Standish RA, Cholongitas E, Dhillon A, Burroughs AK, Dhillon AP. An appraisal of the histopathological assessment of liver fibrosis. *Gut* 2006; **55**: 569–78.
9 Calvaruso V, Burroughs AK, Standish R *et al.* Computer-assisted image analysis of liver collagen: Relationship to Ishak scoring and hepatic venous pressure gradient. *Hepatology* 2009; **49**: 1236–44.
10 Goodman ZD, Becker RL Jr, Pockros PJ, Afdhal NH. Progression of fibrosis in advanced chronic hepatitis C: Evaluation by morphometric image analysis. *Hepatology* 2007; **45**: 886–94.
11 Goodman ZD, Stoddard AM, Bonkovsky HL *et al.* HALT-C Trial Group. Fibrosis progression in chronic hepatitis C: Morphometric image analysis in the HALT-C trial. *Hepatology* 2009; **50**: 1738–49.
12 Lazzarini AL, Levine RA, Ploutz-Snyder RJ, Sanderson SO. Advances in digital quantification technique enhance discrimination between mild and advanced liver fibrosis in chronic hepatitis C. *Liver Int* 2005; **25**: 1142–9.
13 McHutchison J, Goodman Z, Patel K *et al.*; Farglitizar Study Investigators. Farglitazar lacks antifibrotic activity in patients with chronic hepatitis C infection. *Gastroenterology* 2010; **138**: 1365–73. 1673 e1–2.
14 O'Brien MJ, Keating NM, Elderiny S *et al.* An assessment of digital image analysis to measure fibrosis in liver biopsy specimens of patients with chronic hepatitis C. *Am J Clin Pathol* 2000; **114**: 712–18.
15 Wright M, Thursz M, Pullen R, Thomas H, Goldin R. Quantitative versus morphological assessment of liver fibrosis: Semi-quantitative scores are more robust than digital image fibrosis area estimation. *Liver Int* 2003; **23**: 28–34.
16 Masseroli M, Caballero T, O'Valle F, Del Moral RM, Perez-Milena A, Del Moral RG. Automatic quantification of liver fibrosis: Design and validation of a new image analysis method: Comparison with semi-quantitative indexes of fibrosis. *J Hepatol* 2000; **32**: 453–64.
17 Hui AY, Liew CT, Go MY *et al.* Quantitative assessment of fibrosis in liver biopsies from patients with chronic hepatitis B. *Liver Int* 2004; **24**: 611–18.
18 Shikata T, Skai T. Elastogenesis in the liver. *Acta Pathol Jpn* 1974; **24**: 21–31.
19 Scheuer PJ, Maggi G. Hepatic fibrosis and collapse: Histological distinction by orecin staining. *Histopathology* 1980; **4**: 487–90.
20 Thung SN, Gerber MA. The formation of elastic fibers in livers with massive hepatic necrosis. *Arch Pathol Lab Med* 1982; **106**: 468–9.
21 Bedossa P, Lemaigre G, Paraf F, Martin E. Deposition and remodelling of elastic fibres in chronic hepatitis. *Virchows Arch A Pathol Anat Histopathol* 1990; **417**: 159–62.
22 Gilbertson JR, Ho J, Anthony L, Jukic DM, Yagi Y, Parwani AV. Primary histologic diagnosis using automated whole slide imaging: A validation study. *BMC Clin Pathol* 2006; **6**: 4.
23 Glatz-Krieger K, Glatz D, Mihatsch MJ. Virtual slides: High-quality demand, physical limitations, and affordability. *Hum Pathol* 2003; **34**: 968–74.
24 Weinstein RS, Graham AR, Richter LC *et al.* Overview of telepathology, virtual microscopy, and whole slide imaging: Prospects for the future. *Hum Pathol* 2009; **40**: 1057–69.
25 Diamond J, Anderson NH, Bartels PH, Montironi R, Hamilton PW. The use of morphological characteristics and texture analysis in the identification of tissue composition in prostatic neoplasia. *Hum Pathol* 2004; **35**: 1121–31.
26 Hashiguchi A, Hashimoto Y, Suzuki H, Sakamoto M. Using immunofluorescent digital slide technology to quantify protein expression in archival paraffin-embedded tissue sections. *Pathol Int* 2010; **60**: 720–25.
27 Puppa G, Risio M, Sheahan K *et al.* Standardization of whole slide image morphologic assessment with definition of a new application: Digital slide dynamic morphometry. *J Pathol Inform* 2011; **2**: 48.
28 Sertel O, Kong J, Shimada H, Catalyurek UV, Saltz JH, Gurcan MN. Computer-aided prognosis of neuroblastoma on whole-slide images: Classification of stromal development. *Pattern Recognit* 2009; **42**: 1093–103.
29 Gonzalez RC, Woods RE. Object recognition. In: Gonzalez RC, Woods RE, eds. *Digital Image Processing*, 3rd edn. Upper Saddle River, NJ: Pearson Prentice Hall, 2010; 896–9.
30 Zhang YG, Wang BE, Wang TL, Ou XJ. Assessment of hepatic fibrosis by transient elastography in patients with chronic hepatitis B. *Pathol Int* 2010; **60**: 284–90.

SUPPORTING INFORMATION

Additional Supporting Information may be found in the online version of this article at the publisher's web-site:

Figure S1 Whole slide images (WSIs) of liver biopsies from 38 chronic viral hepatitis patients.

Figure S2 Color classification results for WSIs.